Original Study

Moisés Hernández Cordero*, Andreas Pülz

Modelling Antiquity. Surveying the Private Areas of the Episcopal Palace, Side. Turkey

https://doi.org/10.1515/opar-2019-0025
Received February 27, 2019; accepted July 20, 2019

Abstract: The use of digital techniques is often applied today by archaeologists in the field to get quick and reliable 3D surveys for their research. 3D models and reconstructions are the focus for the use of these techniques. The aim of this paper is to present the methodology employed during the 2018 season, and its combination with that from 2016 on the private areas of the bishop's residence of the Episcopal Palace in the ancient city of Side, Turkey. This paper will focus on the data acquisition process, accuracy of the survey, errors and solutions as well as the workflow-process of the data. The aim is to present a useful workflow to combine surveys at a maximum level of accuracy with already completed surveys. A Total Station (TS) survey, Global Positioning System (GPS) Real Time Kinetics (RTK) survey and Structure from Motion (SfM) are among the techniques used to compile the information later exported into a Computer Aided Design (CAD) and Geographic Information System (GIS) environment. Eventually, viable applications of the data created with such methods that help to formulate a new hypothesis for the ritual and non-ritual areas will be shown: plans, 3D models, digital elevation models (DEM) and orthophotos.

Keywords: Early Christianity, Structure from Motion, urban survey, RTK-GPS, geoid model

1 Introduction

The ancient city of Side is located in the Roman province of Pamphylia. Due to its position on the seashore and its harbour, the city became an important trade centre flourishing especially from the Roman period up to early Byzantine times. During the late Middle Byzantine period the city was progressively abandoned. That is why there are no traces of settlement strata from the late Byzantine period until the late 19th/early 20th centuries, when the site was partially occupied by a modern village called Selemiye. From the 1970s onwards, the area became a hub of the Turkish tourism industry with extensive parts of the peninsula covered by huge hotel complexes.

The archaeological research at Side has a longstanding history of 70 years. In particular, A. M. Mansel, one of the most important Turkish archaeologists of the 20th century, studied the ancient city between the 1940s and the 1970s. He uncovered numerous private, public, religious, and secular monuments from the early Byzantine period. However, in alignment with his research interests, his publications mainly included general summaries devoted to the early Christian and Byzantine findings (Mansel, 1963, 1978). Apart from

Article note: This article is a part of the Special Issue on Unlocking Sacred Landscapes: Digital Humanities and Ritual Space, edited by Giorgos Papantoniou, Apostolos Sarris, Christine E. Morris & Athanasios K. Vionis

***Corresponding author: Moisés Hernández Cordero,** Institute for the Study of Ancient Culture (IKAnt), Austrian Academy of Sciences, Vienna, 1020, Austria, E-mail: moises.hernandez.cordero@oeaw.ac.at
Andreas Pülz, Institute for the Study of Ancient Culture (IKAnt), Austrian Academy of Sciences, Vienna, 1020, Austria

Mansel, other researchers have published very important studies on late antique and medieval monuments in Side, such as S. Eyice (Eyice, 1957, 1957a, 1958, 1960), V. Ruggieri (Ruggieri, 1995, 1995a), C. Gliwitzky (Gliwitzky, 2005), U. Peschlow (Peschlow, 2010), and most recently L. Kaderli (Kaderli, 2009), Ş. Yıldırım (Yıldırım, 2013, 2017) and K. Piesker (Piesker, 2017). With regard to the historical and historical-epigraphic studies, it is worth mentioning especially the work of J. Nollé (Nollé, 1993, 2001) and C. Foss (Foss, 1996), as well as that of H. Hellenkemper and F. Hild (Hellenkemper & Hild, 2004).

The research focuses on a 120 m by 210 m area in the north-eastern part of the ancient city uncovered by Mansel (Fig. 1). A majority of researchers accepted Mansel's interpretation of this area as the episcopal quarter of Side (Müller-Wiener, 1989, p. 683; Hellenkemper & Hild, 2004, p. 393; Foss, 1996, p. 41; Ceylan, 2007, pp. 174–176). Nevertheless, there are some scholars who question this interpretation (Gliwitzky, 2005, p. 342; Buchwald, 1984, pp. 226–227).

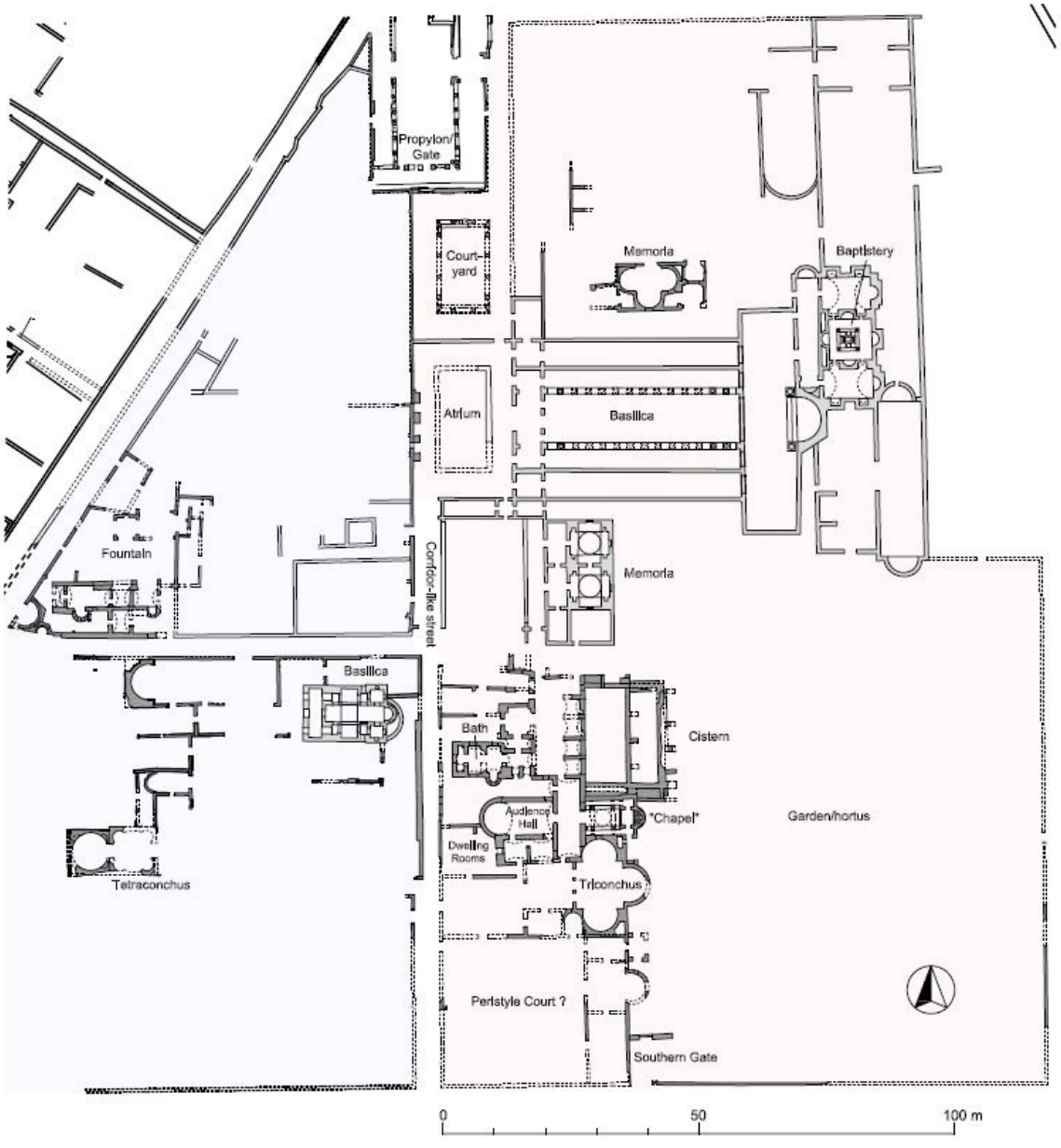

Figure 1. City map, detail with the episcopal district © ÖAW/IKAnt and Excavation Side.

The episcopal quarter was accessed via a propylon/gate at the end of a colonnaded street. The sacral centre, situated in the northern half of the district, showed an approximately 60 m-long three-aisled basilica with corridor-like hallways along the side naves, giving access to a transversely mounted transept. An atrium is located at the western front of the basilica/cathedral, which can most probably be dated to the late 5th or the beginning of the 6th c. AD (Mansel, 1978, pp. 268 and 271 with fig. 302b). In the north-eastern corner of the basilica is a baptistery (Ristow, 1998, p. 251) with a rectangular vestibule and three separate rooms that serve as the *catechumeneum*, baptismal premise, and *consignatorium*.

In the north of the cathedral, a building with an inscribed three-apse room surrounded by walls is preserved within an area of 60 by 60 m. According to the excavator, it is possible to interpret this building as a memorial.

Mansel proposed a similar function for the rectangular building in the south of the basilica. This complex consisted of two domed rooms with an anteroom each. An elongated entrance room in the west connected these two premises, for which a function as a *skeuophylakion* could also be assumed (Hellenkemper & Hild, 2004, p. 392). This further interpretive approach is based on typological parallels of buildings, for example the southern annex building of the basilica in the area of the Roman Imperial temples for Athena and Apollo near the harbour of the city (Mansel, 1978, pp. 257–264).

Figure 2. Episcopal residence, 3D model view to the east © ÖAW/IKAnt (M. Hernandez Cordero).

Numerous premises (Figs. 2 and 3) follow further south of the two-room complex. These include a little bath, which, due to its small dimensions, did not function as a public bath, but as a private *balneum*. To the east, a huge cistern with two rectangular basins is notable (Figs. 2 and 3). Following the bath are the two-storied dwelling rooms of the bishop (Müller-Wiener, 1989, p. 682; Ceylan, 2007, pp. 174 and 176), one of them showing a formerly very rich decoration and an apse in the west (Figs. 2 and 3). This room could be interpreted as the reception/audience hall of the bishop. The anteroom to the east did not serve exclusively as a vestibule of the reception hall but also as a distribution room, connecting the premises in the north and south of this compound. It also served as the *narthex* of a small, three-aisled church, which was characterized by a central dome supported by four columns (Gliwitzky, 2005; Yıldırım, 2017). This richly decorated building was most probably not part of the early Byzantine residence but rather a later addition (Fig. 3). In fact, the chronology of the church is very difficult to define. While the excavators and various scholars suggested a date during early Byzantine times (contemporary with the residence), a medieval dating has also been proposed (cf. the overview of the different chronological approaches in Yıldırım, 2017, pp. 423–425).

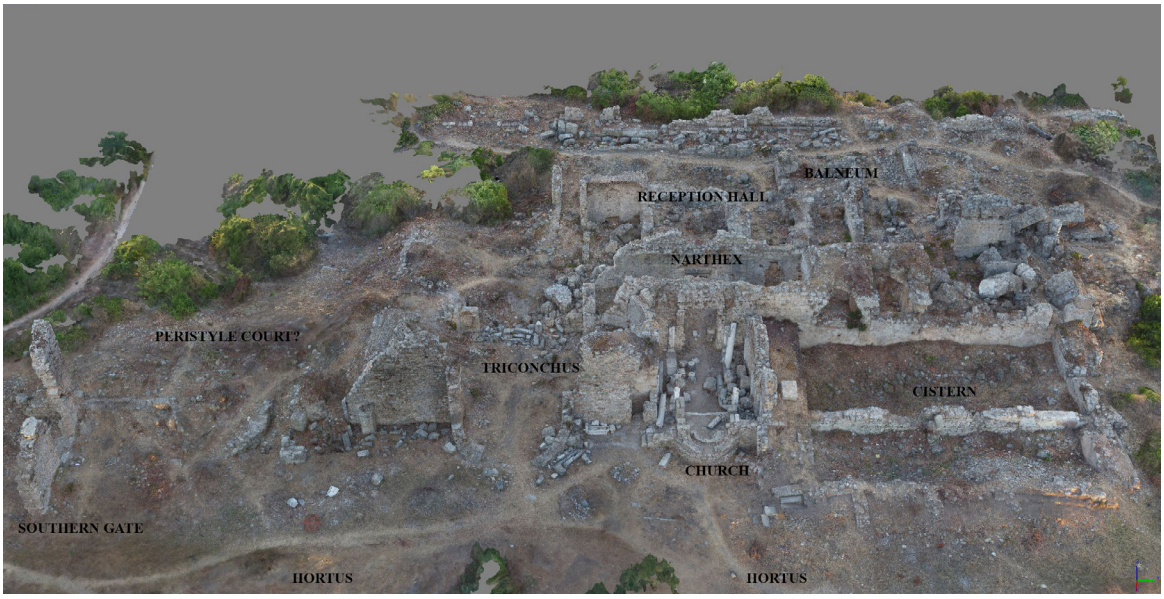

Figure 3. Episcopal residence, 3D model view to the west © ÖAW/IKAnt (M. Hernandez Cordero).

Finally, south of the living quarters and the church, a huge triconchus (most probably the *triclinium*) is preserved. The main room with its trifold apses in the east was accessible from an almost square *vestibulum* in the west. The door between the two rooms was constructed with Roman marble blocks and designed as a *tribelon*. Next to this building, another complex with several premises followed, one of them having an east-facing apse. As the research stands at present, an interpretation of this partly excavated building is not possible.

On the south-eastern side of this complex, a monumental gate gave access to an undeveloped area (Fig. 1). Due to the absence of buildings, the first excavator proposed an interpretation as a *hortus*, surrounded by an enclosure wall (Mansel, 1978, p. 282; for the results of the geophysical investigations cf. İ. Akca & A. Pülz, 2018). Almost all scholars suggest that the entire episcopal complex ends with a narrow, 4 to 5 m-wide corridor-like street on its western edge.

Starting in 2015, the project investigations aimed to understand the function and architectural history (dating, duration of use, and construction style) of the episcopal district with the cathedral, various memorials, the residence, two courtyards, the garden, etc. As per the previous data, these monuments would cover an area of about 120 m by 210 m. However, within the recent research some new information has been found, indicating that the episcopal district possibly also included the triangle-shaped sector west of the area (Fig. 1: red-interlaced resp. blue-interlaced area). In this case, the episcopal district would have had an extension of about 3.6 ha and, consequently, it would have been one of the largest of the entire early Byzantine *oikumene* (cf. the list of episcopeia and their land occupancy in Müller-Wiener, 1989, p. 703).

2 Method

This chapter will focus on the methodology used during the 2018 campaign. The description of the creation of the 2016 ground control points (GCPs) has already been discussed in another publication (Hernández Cordero, 2017, pp. 457–460), but it will be referred to here when necessary. As a summary of that campaign, the survey job pursued the setting up of a workflow in order to generate, by the end of each season, a complete 2D and 3D survey of the remains. A geomatics approach was adopted in order to fulfil the three main objectives of the survey: accuracy, flexibility, and speed. The work focused on the creation of a GCP network without any known point. It was possible to create an accurate and dense network of points in both a local coordinate system and the Turkish National Reference Frame (TUREF), using a combination of TS and GPS-RTK (Hernández Cordero, 2017, p. 460).

By contrast, the 2018 campaign sought to improve the creation of the point network and its integration into the TUREF. The aim was to use the GPS-RTK Turkish network TUSAGA-Aktif to survey main structures, and also to obtain orthometric heights for the archaeological record. The methodology applied pursued three main objectives:

- more extensive use of the RTK TUSAGA-Aktif Turkey network for surveying the archaeological structures and creation of the GCPs (specially for SfM), and speeding the capturing of the data with an accuracy of ±0.02 m horizontal and ±0.03 m vertical;
- to resurvey the GCPs already collected during 2016 in order to integrate them into the 2018 survey campaign, converting the ellipsoidal heights into orthometric ones, and re-processing the 2016 SfM data to combine the information from both campaigns in the future (as shown on the orthophoto in Fig. 8 and the DEM in Fig. 10);
- to adapt the 2016 survey (TUREF WGS84 and local coordinates) and the one for 2018 (TUREF WGS84 with orthogonal heights) to the coordinate system in our CAD file (ED50/TM30). This would allow for a reliable workflow that allows for switching between coordinate systems with the minimum displacement and error possible. It will therefore be possible to revert from the two coordinate systems to a local one.

RTK-technology has been used in archaeology before, as a tool for capturing points in the field (Scianna & Villa, 2011, pp. 353–354; Grau Mira, 2016, p. 4), and more recently to capture targets used in photogrammetric surveys (Roosevelt 2014, p. 32; Ostrowski & Hanus, 2016, p. 975; Chiabandro et. al., 2016, p. 31). Notwithstanding its relevance for data capturing, its significance and potentiality makes it possible to expand its use through diverse but related methodologies.

2.1 Geoid Model Creation

Yilman & Karaali (2010, p. 1829) state that "a geoid surface is the closed surface going under the land which coincides with stable sea surface". Due to gravity anomalies on the Earth's surface, the geoid surface is more irregular than the ellipsoid one, so is often used to get the closest value to the Earth's physical surface (Sanlioğlu et al., 2009, p. 2) (Fig. 4). The geoid undulation is the separation between the ellipsoid reference and the geoid surface (Heiskanen & Moritz, 1967, p. 292) and can vary by ±85 m and ±106 m worldwide (Okiwelu, Ajuma & Okwueze, 2011, p. 9).

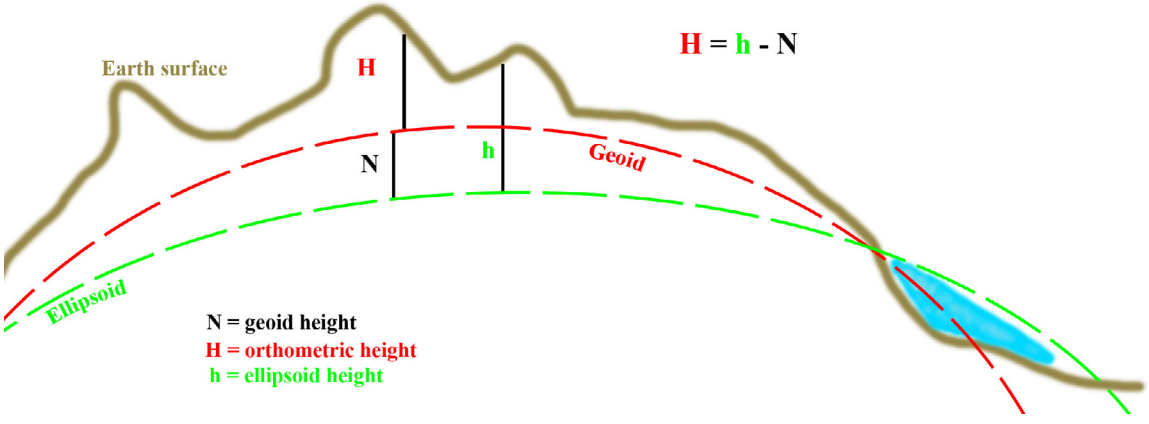

Figure 4. The relationship between heights systems © M. Hernández Cordero.

Turkey uses a hybrid geoid model-2009 (THG-09) computed using the Earth Gravitational Model 2008 (EGM08), calculated from satellite altimeter measurements and surface gravity measurements (Aktuğ et al., 2010, p. 7; Kiliçoğlu et al., 2010, p. 571; Yilmaz, 2013, p. 27). The orthometric heights are calculated using the equation: N = h – H (Heiskanen & Moritz, 1967, p. 328) (Fig. 4). As the details for the THG-09 were not available, we had to create a local transformation in our area of intervention to get the orthogonal heights and generate a local geoid model. Typically the heights measured by GPS technology are ellipsoidal (Sanlioğlu, Maras, & Uysal, 2009, p. 3); consequently they need to be transformed into orthometric ones before they can be used for archaeological recording.

The selected method is the "Twostep transformation" in Leica software which is included in Leica Geo Office (Leica Geosystems, 2018a, p. 61), SmartWorx Viva (Leica Geosystems, 2016, pp. 700–704) and Captivate software (Leica Geosystems, 2018, p. 510). This transformation was favoured due to three main factors:

- the unavailability of the THG-09 parameters for our GPS,
- the area being surveyed may be extended in the future,
- other methods are not suitable for areas in excess of 10 km^2 (e.g., the one-step method) and does not take into account the geoid undulations.

There are other survey software programs with similar features, like LISCAD on Transformation Projection, or MicroSurvey with the Helmert Transformation (MicroSurvey Inc, 2018, p. 244); however, after a careful examination it was concluded that the Leica transformation met the requirements for our fieldwork survey.

The aforementioned "Twostep transformation" is designed to cover areas not bigger than 100 km^2. In order to acquire better results, the distribution of reference points must surround the working area. These points (with the known coordinate system and height) are matched in the software with the points captured using the Global Navigation Satellite System (GNSS) sensor. It is crucial that the local projection and local ellipsoid of the coordinates with the orthogonal heights are known, otherwise only the one-step method can be adopted (Leica Geosystems, 2014, p. 3). The biggest coordinate correction must be not greater than ±0.140 m (Table 1) per point, which is the maximum displacement accepted when using this technique (Ersoy, 2011, p. 8005), and acceptable for the current needs of our project. The GPS and TS measurements are not affected, as the transformation is only used for the 11 key ground control points used for the conversion. In the process, the corrections are distributed equally across the surface (Başçiftçi, Çağl, Ayten, Akkuş, Yalcin, & Şanlioğlu, 2006, p. 4). This equal distribution is of utmost importance within the process, as the residual error per point is calculated taking into account the entire surveyed surface (see Table 1). The calculation may not be exact, but it is accurate enough for most practical applications in surveying (Yilmaz, Turgut, Gullu, & Yilmaz, 2016, p. 19).

Once on site, for the capture of the data and the subsequent calculation of the geoid model we used the Leica CS15 controller, with the Viva software and the GS14 GNSS antenna. Using a wooden tripod to improve the accuracy (Wisconsin Department of Transportation, 2017, p. 6) and 50 readings per point, a total number of 11 GCPs were recorded with an accuracy error of ±0.020 m horizontal and ±0.030 vertical. In our case, the points used are survey nails fixed on concrete blocks or on the pavement, that are distributed along the streets and archaeological areas of Side. They were located using a previous survey on a CAD file. This step demands an *in situ* control of the quality of the GCPs, as it is essential to monitor whether they are still intact and firm on the ground. Of the 105 points located in the CAD file, only the 11 used for the transformation met the requirements for the process. As there is no study stating that a minimum number of points is necessary for the transformation, and since it was not possible to locate more of them on site, we decided to continue the workflow. To ensure quality data, the points were surveyed on the same day, trying to ensure good satellite coverage (Pirti, 2010, p. 25; Wisconsin Department of Transportation, 2017, p. 1), similar weather conditions, and a connection to the same RTK base. On a positive note, no drop off in the connection with either the RTK network or the satellites occurred during the three hours spent walking across the site.

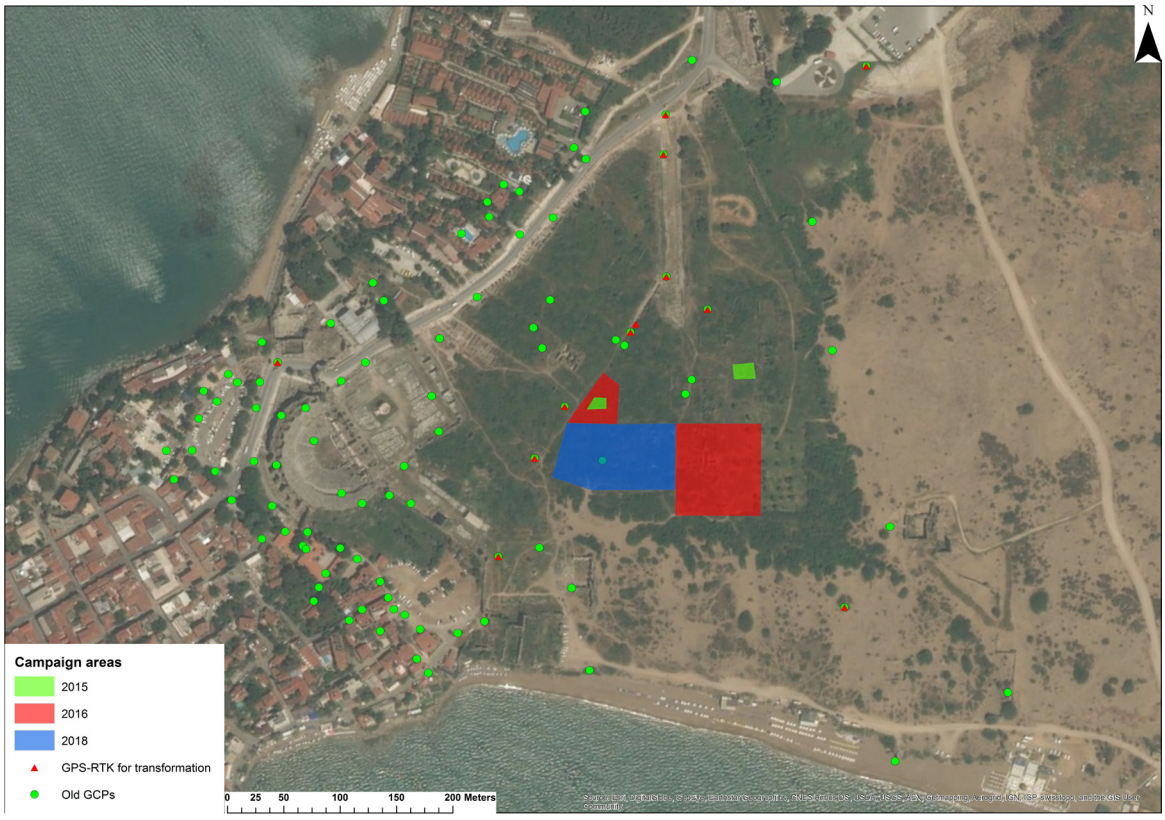

Figure 5. Campaign areas and GCPs used for transformation © ÖAW/IKAnt (M. Hernández Cordero).

2.2 TS and GPS Survey

A combination of TS and GPS-RTK survey was selected to set up the stations and to collect the retro targets forming the ground control network. This method is the most prominent among those used to create control points (Schofield & Breach, 2007, p. 24). We employed the open traverse technique for the positioning of the stations across the field, in order to reach every corner of the research area (Fig. 6). Different Electronic Distance Measuring (EDM) options were used to capture the location of the targets, the location of the new stations, and the geometry of the archaeological remains. The measurements were processed using Leica Geo Office 8.4 and LISCAD 2018.

As the observation distance should not exceed 500 m when measuring with TS (Ersoy, 2011, pp. 8005–8006), the GPS-RTK survey is a sound alternative to the TS survey in large areas. It provides accurate data to the surveyor in real time (Roosevelt, 2014, p. 32), and it is a very good general observation tool for determining the survey coordinates, horizontal and vertical, of a point (Wisconsin Department of Transportation, 2017, p. 6). The development of this technology enables surveyors to coordinate marks of interest in a rapid, efficient manner, and is appropriate for any application that requires both high precision and high productivity (Pirti, 2010, pp. 23–24). One of the limitations of RTK connection is to do with the GNSS receivers, as the radio signals have to travel approximately 20,000 km from the Earth (Pirti, 2010, p. 25). The critical factor here is to check the satellite window, with 5-10 satellites visible and available in the RTK surveying.

Most of the structures were surveyed with the RTK network, so there was no need to post-process the data (Schofield & Breach, 2007, p. 351).

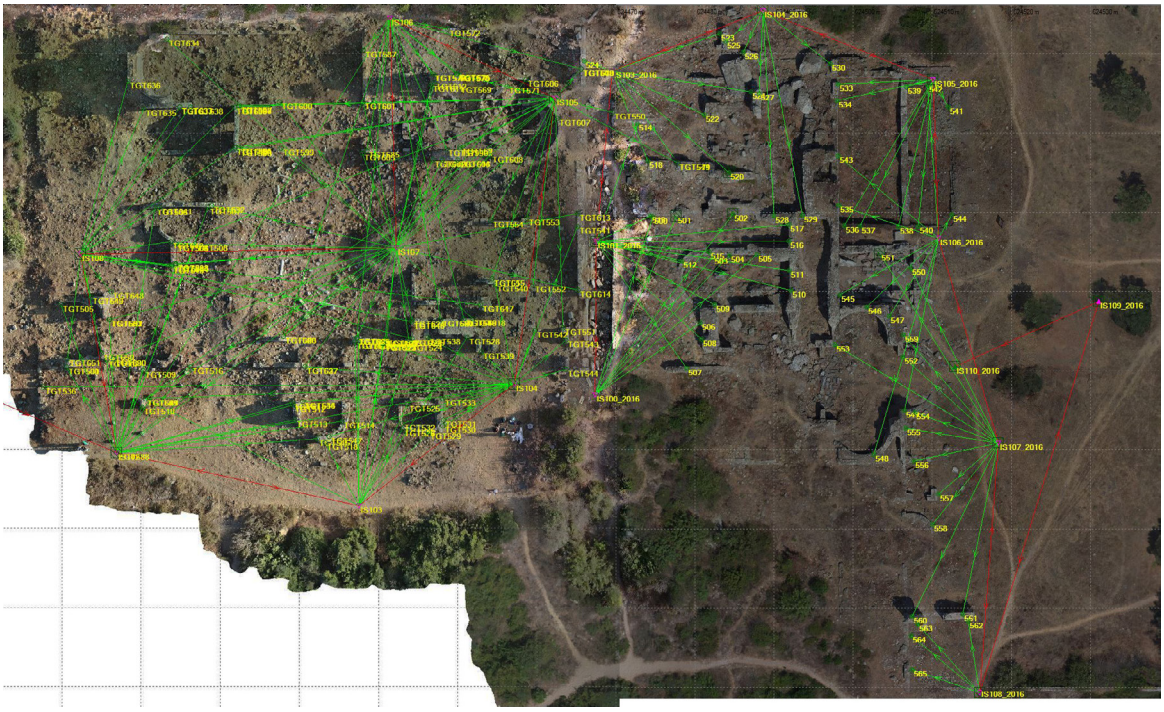

Figure 6. 2016/2018 GCPs network over an orthomosaic generated in Agisoft Photoscan 1.4.4 © ÖAW/IKAnt (M. Hernández Cordero).

2.3 SfM Data Capture

To enhance the 3D survey accomplished with the TS and the GPS, we also undertook a photogrammetric survey with both a drone and a digital single-lens reflex (DSRL) camera. The use of the SfM technique was settled upon due to its tested utility and accuracy on archaeological projects (Doneus, Verhoeven, Fera, Briese, Kucera, & Neubauer, 2011, p. 87; Lo Brutto & Meli, 2012, p. 6). In 2016 acquisition of the image data, which had a resolution of 4000 x 2250 pixels, was achieved using a DJI Inspire I with a DJI Zenmuse X5 camera and a DJI MFT 15mm objective. The focal length used alternated between 2.3 to 4.0, a decision determined by the location of the drone, the target to be captured (wall or ground) and the time of day (for the light conditions). By contrast, in the 2018 campaign the photo capture was done using a Canon EOS 70D, with a Canon EF 35 mm stabilizer objective mounted on a 4 m photo pole and 5472 x 3648 pixels (see Fig. 7). The chosen focal length now ranged between 2.8 and 3.5. The advantage of the DSLR cameras is that they can be used to accurately reconstruct scene geometry in SfM (Burns, Delparte, Gates, & Takabayashi, 2015, pp. 2–3) as well as to export data without any additional post-processing (Jaud, Passot, Le Bivic, Delacourt, Grandjean, & Le Dantec, 2016, p. 7): general models of the area (Figs. 2 & 3), high-quality dense point clouds, very detailed orthomosaics of the remains (e.g., for elevations) and DEM (Fig. 8).

During both campaigns, the photos were captured at dawn and dusk to avoid, as far as possible, significant changes in the environmental conditions (Tola, Knorr, Imre, & Alatan, 2005, p. 2) by means of having a consistent level of light (Michelleti, Chandler, & Lane 2015, p. 4). This procedure facilitates the subsequent processing of the images as well as the creation of a uniform texture map. As per the generation of the DEM, we used the photos taken by a DJI Mavic drone with a resolution of 1280 x 960 pixels, provided on site by Turkish colleagues.

Part of the processing took place on site, working with a fieldwork laptop – i7-4710HQ 2.50 GHz, 16 GB RAM and a NVIDIA Geforce GTX 860M – in order to check coverage of the captured areas. For the processing of all SfM data in the office, an Ubuntu-Linux server cluster with 6 nodes was used in order to have enough computer power. Each node has a 2x Intel Xeon E5-2650 v4 (Broadwell-EP) 12-Core CPU processor with 512 GB RAM, and 2 NVIDIA Geforce 1080 GTX Ti, 11GB.

Figure 7. SfM data capture on mast/pole © ÖAW/IKAnt (A. Pülz).

3 Results

The results presented in this paper are not conclusive, as the processing of some of the data is still in progress due the quantity and size of some of the files (e.g., the 232 GB for the exported high dense point cloud for the 2016–2018 campaign). Nevertheless, what has already been accomplished needs to be mentioned, as well as its usefulness in improving the associated research project.

3.1 Geoid and Survey

The calculation of the geoid transformation was done on site, after collection of the information from the 11 GCP points still remaining. They covered an area of 138,000 m^2 (Fig. 5). It is common that errors in the geoid calculation appear, as mistakes are produced when matching the points or due to misidentification of coordinates on the GCP list. Consequently, it is advisable to keep a clear record for every point in order to avoid mismatches during the transformation process.

It has been mentioned that due to the lack of a THG-09 geoid model, it was not possible to test the displacement. In that case, a dependence on the existent bibliography and works where this technique was used is mandatory in order to apply this method.

A total number of 9 stations was used for the open traverse on site. 153 retro targets were surveyed with an accuracy of ±0.003 m horizontal and vertical, generating a dense network of GCPs in an area of 11,000 m^2. Up to 5 other stations were set up in the field with the resection method using the processed retro targets. These points would also help in the georeferencing and the improvement in accuracy of the SfM data (Verhoeven, Doneus, Briese, & Vermeulen, 2012, pp. 2062–2063). A combined GCP network, containing 23 stations and 197 GCPs from the 2016 and 2018 campaigns, was then calculated (Fig. 6).

Plans of the working area were generated daily on AutoCAD, thus supporting the selection of strategies to follow on the ensuing day. A general plan of all the surveyed archaeological features on the TUREF coordinate system was implemented after the fifth day (Fig. 11). A final plan of the surveyed area will contain the researcher's documentation as well as the types of remains and the shape of the structures.

Table 1. Leica Geo Office results for Twostep transformation © ÖAW/IKAnt (M. Hernández Cordero).

System A	System B	Easting	Northing	Position	Height	Position + Height
15	15	0.0745	0.0093	-0.0335	0.0751	0.0822
18	18	0.0066	-0.0178	-0.0428	0.0189	0.0468
19	19	-0.0450	-0.0094	0.0299	0.0459	0.0548
20	20	0.0024	-0.0757	-0.0368	0.0757	0.0842
21	21	-0.1024	-0.0566	-0.0183	0.1170	0.1184
31	31	0.0458	0.0323	-0.0044	0.0560	0.0562
1180	1180	0.0126	0.0114	0.0293	0.0170	0.0338
1185	1185	0.0083	0.0156	0.0174	0.0176	0.0248
3257	3257	-0.0404	0.0414	0.0176	0.0578	0.0604
3516	3516	0.0233	0.0259	0.0518	0.0348	0.0624
3519	3519	0.0142	0.0236	-0.0102	0.0276	0.0294

Table 2. Graphical overview of the Twostep transformation residuals © ÖAW/IKAnt (M. Hernández Cordero).

No.	dE [m]	dN [m]	dHgt [m]
1180	0.0126 m	0.0114 m	0.0293 m
1185	0.0083 m	0.0156 m	0.0174 m
15	0.0745 m	0.0093 m	-0.0335 m
18	0.0066 m	-0.0178 m	-0.0428 m
19	-0.0449 m	-0.0094 m	0.0299 m
20	0.0024 m	-0.0757 m	-0.0368 m
21	-0.1024 m	-0.0566 m	-0.0183 m
31	0.0458 m	0.0323 m	-0.0044 m
3257	-0.0404 m	0.0414 m	0.0176 m
3516	0.0233 m	0.0259 m	0.0518 m
3519	0.0142 m	0.0236 m	-0.0102 m

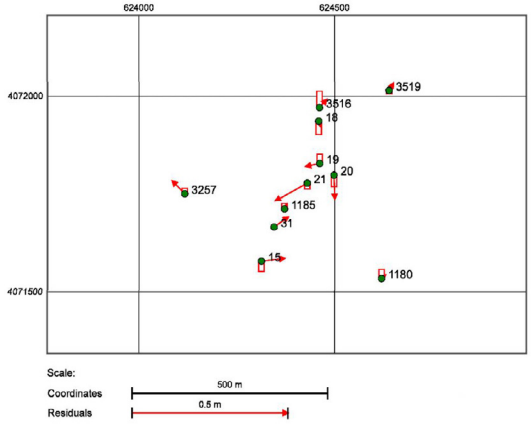

3.2 SfM

The SfM data was processed on Agisoft Photoscan 1.4.4 following the standard procedures described by other authors (Kowlessar et. al., 2019, p. 480; Michelleti et. al., 2015, pp. 4–6; Mercer & Westbrook, 2016, pp. 2902–2904). All the files (2016 and 2018) have been georeferenced using the last version of our surveyed GCP network on TUREF/TM30 (EPSG:5224). Following the quality control and the discarding of the instances with a lower quality (less than 0.70 in Agisoft), 5421 images were processed from the 2018 season. A dense point cloud was generated in 8 hours in order to identify any gaps in the data (high alignment accuracy-generic preselection, medium dense point cloud quality).

The workflow also sought to integrate the SfM data into one main Agisoft file, bringing together the photos captured from diverse cameras: DJI Zenmuse 5X (season 2016) and Canon EOS 70D (season 2018). The alignment and high dense point cloud generation of the 2016 and 2018 datasets with a quality control threshold of 0.70 (10,000 images) took 128 hours (medium alignment accuracy, high dense point cloud quality). However, because of the size of the dataset and the size of the point cloud (2.5 billion points),

the calculation of the final mesh and texture map is still in progress. The size of the dataset caused a few problems with the software, making it crash with "index overflow" errors, probably because of the high density point cloud. A solution consisting in the division of the data using Python scripts, proposed by the Agisoft company, so-called "split in chunks" (Agisoft LCC, 2017), is being tested. The script works so far, but the alignment of the divided data into a big mesh chunk is not showing all the data.

Several files were exported from these processed datasets and used in other software (CloudCompare and ArcGIS), generating additional information for the project:

Point Clouds: Dense point clouds were imported into AutoCAD to complete some areas of the general plan and the vectorization of wall elevations (Hernández Cordero, 2017, p. 461). On 3D Studio Max, they are being used for the 3D reconstruction of the buildings for a visualization of the episcopal compound. Currently, we are using point clouds and no meshes because the quantity of faces generated (from 40 mill. to 128 mill.) arguably makes it hard to import it with that quality on CAD or 3D software (3D Studio Max, Blender). Also, the point clouds are lighter and easy to decimate or slice into areas without losing quality.

DEM: Two DEM were calculated. The first one is a raster file of 5,103 x 4,313 pixel size from 265 images captured during the 2018 campaign with the DJI MAVIC and the following parameters: high accuracy alignment-non generic preselection, ultra-high dense point cloud quality, arbitrary surface type and high face counting for the mesh. The second one (Fig. 8) with 330 photos (1260 x 860 pixels from the DJI MAVIC and 4000 x 2250 pixels from the DJI Zenmuse X5) resulted in a DEM of 25,001 x 19,130 pixel size. In this case, the parameters were: highest accuracy alignment-non generic preselection, high dense point cloud quality, arbitrary surface type and high face counting for the mesh (Figs. 9.1, 9.2, 9.3 and 9.4).

Figure 8. 2016 and 2018 field campaigns survey and DEM generated in Agisoft Photoscan 1.4.4 © ÖAW/IKAnt (M. Hernández Cordero).

Figure 9.1. Point cloud view (© M. Hernández Cordero).

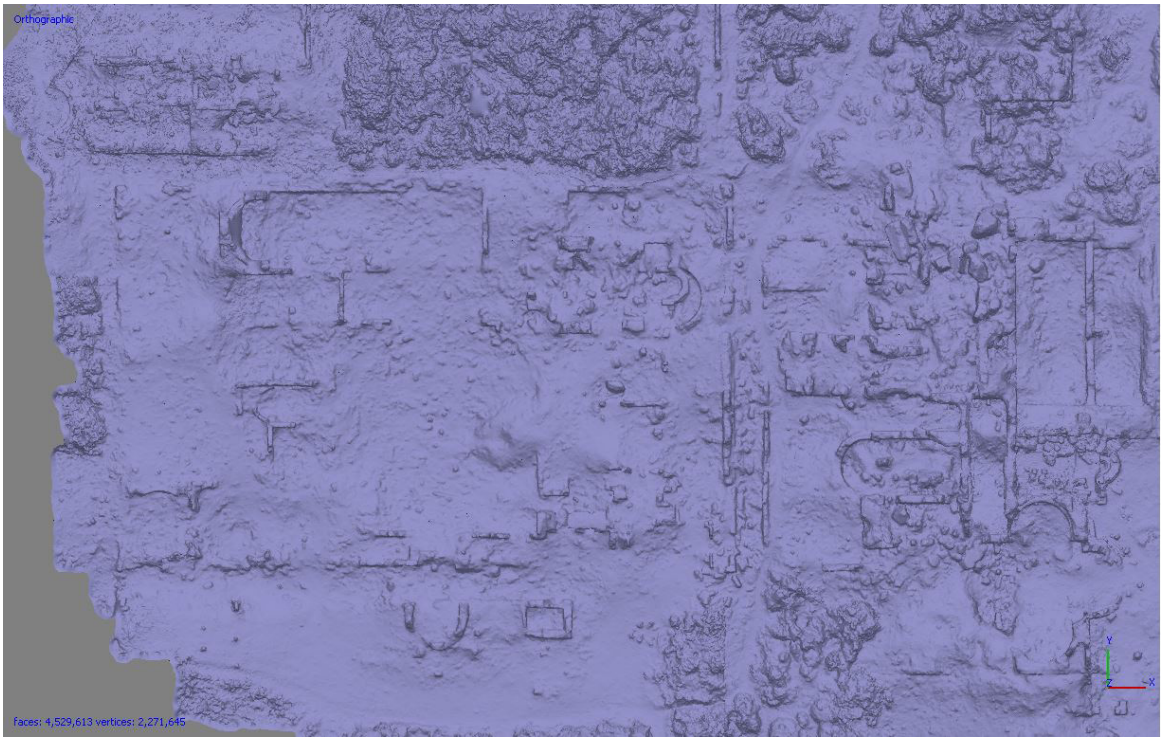

Figure 9.2. TIN view (© M. Hernández Cordero).

Figure 9.3. Textured model view (© M. Hernández Cordero).

Figure 9.4. DEM view (© M. Hernández Cordero).

The SfM RMS reprojection error is 0.314188 and the total error of the GCP used (2016 and 2018 together) is 0.089320 (Table 3).

Table 3. Agisoft PhotoScan calculated errors between the GPS control point positions and the positions calculated for the same points in the 3D model generated (© M. Hernández Cordero).

Label	X_error	Y_error	Z_error	Error_(m)	Projections
2016 targets					
target_1190	-0.007560	-0.058606	0.008571	0.059710	5
target_IS110	-0.029452	0.014818	-0.019458	0.038283	8
target37	-0.055323	0.016339	0.070718	0.091261	16
target39	-0.017907	0.091294	0.103389	0.139084	10
target40	-0.016179	-0.031066	0.012122	0.037065	7
target68	0.023818	0.051881	-0.012146	0.058365	4
target71	-0.036134	-0.084086	0.018366	0.093346	7
target78	0.019934	-0.024379	-0.078078	0.084189	14
target158	-0.002407	0.025132	0.060780	0.065815	13
target181	-0.036293	0.076710	-0.117006	0.144540	8
target197	0.030095	-0.005740	0.001784	0.030689	4
target198	0.039003	-0.017879	-0.059933	0.073708	6
target199	0.031009	-0.061846	-0.008332	0.069684	3
2018 targets					
TGT700	-0.003618	-0.052839	0.016581	0.055497	6
TGT701	0.049013	0.127927	0.005371	0.137100	6
TGT702	0.022656	-0.093105	0.012885	0.096685	3
TGT703	0.018046	0.076538	-0.071596	0.106347	3
TGT704	-0.026725	-0.014579	-0.078181	0.083899	9
TGT705	-0.055654	0.226102	-0.110795	0.257867	14
TGT706	0.040631	0.040782	0.069869	0.090530	16
TGT707	-0.042379	-0.077714	0.064939	0.109784	4
#Total error	0.030794	0.061591	0.056889	0.089320	

Orthophotos: In 2016 we generated several orthophotos for the vectorization of the walls, as well as an aerial view of the episcopal residence (Hernández Cordero, 2017, p. 461). After the 2018 campaign, a general 20,502 x 15,264 pixel orthomosaic of the project was computed. Using the aforementioned photos for the DEM, the parameters selected were: high accuracy alignment-non generic preselection, ultra-high dense point cloud quality, arbitrary surface type, high face counting for the mesh, and blending mode mosaic with 0.0105924 pix for the orthomosaic (Fig 10).

Figure 10. 2016 and 2018 field campaigns survey orthomosaic generated in Agisoft Photoscan 1.4.4 © ÖAW/IKAnt (M. Hernández Cordero).

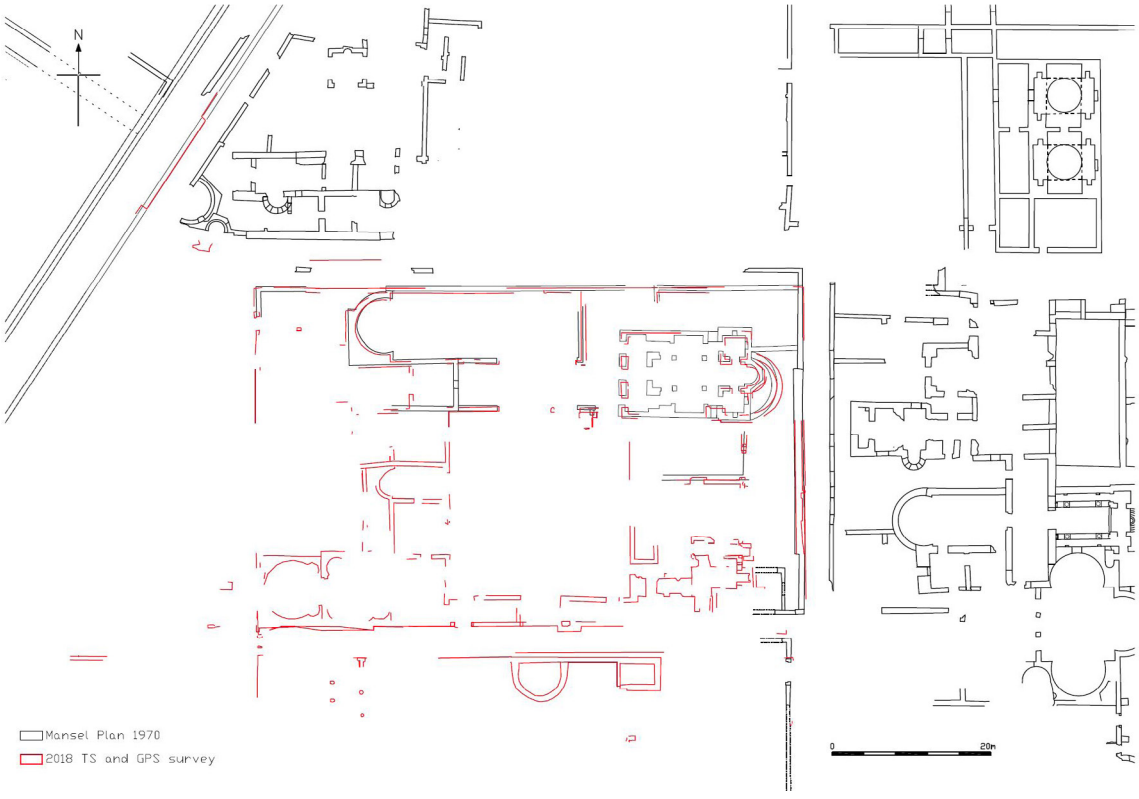

Figure 11. TS and GPS-RTK 2018 survey together with previous interventions © ÖAW/IKAnt (M. Hernández Cordero).

3.3 Archaeological Information

The documentation work shows the presence of various corridors, gates and doorways that connect the different wings of the episcopal quarter with a 1.4 ha triangle-shaped area in the west (Fig. 10). Perhaps these *insulae* housed further buildings characteristic of episcopal residences, like guesthouses, dwelling rooms for the clergy, premises needed for the practice of caritas, kitchens, pantries, toilets or stables.

In the 2018 survey works, a series of different building remains were documented in the insula immediately west of the little *balneum* (Fig. 1, Fig. 10). Here we can highlight the example of an early Byzantine three-aisled basilica which was replaced by a domed cross-in-square church of middle Byzantine times (Ruggieri, 1995, pp. 106–108; Ruggieri, 1995a, p. 112, Eyice, 1958, p. 42). Furthermore, it may be worth mentioning two square central buildings with four internal apses, each of which encloses two rectangular rooms with apses. Besides this case, there are also some vaulted two-storied premises in the south-eastern corner, as well as a peristyle court in the centre of the insula.

On the northern neighbouring insula a little fountain house, situated in the centre of a courtyard, can be observed (Fig. 11). The northern front wall of the square fountain was decorated with a niche of about 2 m in height. The paintings depict a winged, life-size angel with a haloed head (Pülz, 2018).

4 Conclusions

The 2016 and 2018 survey workflow is intended to support the use of the three techniques referred to here (TS, GPS-RTK, SfM) for the benefit of archaeologists in fieldwork. An immediate positive result from both the 2016 and the 2018 campaigns was the possibility of checking the progress of the survey on the spot, helping in deciding where to focus on the next day. The SfM process in the field supported this decision, as when new possible features like the peristyle courtyard in the middle of our 2018 intervention area and the alley to the south were identified (Figs. 9.4 and 10).

The methodology developed in this project conceives moving from local, regional, and national to a worldwide coordinate system. Such systems have different scales that can be linked together accurately through this method (Campana, Sordini, & Remondino, 2008, p. 2). Furthermore, our GCPs can be linked to local surveys for small interventions, medium urban building survey projects (like our project) or regarding the hinterland of the settlement.

The local geoid model transformation has granted us the opportunity to use old plans from Mansel (Mansel, 1963), old GPS surveys with no metadata information, and CAD drawings with missing geodata (e.g., ED50/TM30 CAD plan in our project). This is a valuable corollary, as archaeologists reuse data directly from other archaeologists but access to metadata can be poorly preserved or simply not available (Faniel, Kansa, Whitcher Kansa, Barrera-Gomez, & Yekel, 2013, pp. 6–7). With this approach, only few geographic data need to be known and, together with the TS-GPS-RTK survey plans created in previous projects, these can be used and local transformations for geolocation undertaken.

The accuracy of the survey is crucial for the successful development of the project. The project is still ongoing and is planned to last several years. The link between georeferenced data from former and future fieldwork campaigns needs to be matched as faultlessly as possible. One of the disadvantages is that the SfM data needs to be aligned in Agisoft in one chunk in order to generate the most accurate 3D model possible. Thus, with more data being added each year, the processing of this one chunk can prove a problem. The plan is to use better and more powerful hardware (referenced below) while the possibility of generating 3D data from small features (e.g., rooms, alley-ways, fountains) with enough accurate GCPs to generate an accurate model is a must. Elevations, plans, and a DEM of the areas must be based on a georeferenced network of reliable GCPs, to minimize as far as possible the mismatch when data from more than one campaign is used for archaeological analysis.

Two weeks of fieldwork allowed for the testing of the speed and precision of the methodology presented. No gaps or missing information on the data occurred, so it can be concluded that the TS/GPS survey as well

as the photographic capture for SfM, worked as expected. A plus is that the work could be undertaken employing only a technician, including the use of the traverse technique. It must be noted that TS and RTK GNSS survey is not easy for an untrained technician to implement (Roosevelt, 2014, p. 40), so it must be borne in mind that its implementation necessitates qualified personnel.

The 3D SfM data generated every day in the field served as a useful tool for visually representing the physical characteristics of the working area (as already mentioned by Burns et al., 2015, p. 12), bringing other perspectives to the archaeologists undertaking the fieldwork. This research has demonstrated the strengths of the 3D approach when implemented on an ancient urban site such as Side. Moreover, it concurs with other researchers' opinions (Dell'Unto et al., 2015; Kowlessar, Benjamin, Moffat, & Van Duivenvoorde, 2019, p. 487) regarding its utility in understanding large, complex, and visually complicated environments. However, in future applications it would be interesting to use 3D data as a dataset, itself to be queried as in other works (Auer, Agugiaro, Billen, Loos, & Zipf, 2014). Thus, the use of Agent Base Modelling (ABM) to explore the use of the episcopal quarter, querying the building environment (Crooks, Hudson-Smith, & Patel, 2011, p. 56; Crawford, 2019, p. 318), would be of special interest. The importance of each area and the most prominent buildings can be weighted in the software, in order to see if they actually structure the surrounding urban framework.

The amount of 3D data generated has confirmed that an improvement in the workflow is advisable, in order to make it less consuming in terms of time (like the SfM server processing) as well as economic resources. A manageable option would be the use of non-proprietary software for capturing the data, avoiding the cost of licenses like Leica Geo Office, LISCAD or the Viva SmartWorx. Additionally, in order to simplify the more common tasks, some steps in the workflow could use more programming/scripting language: moving file photos, selecting quality photos, and deleting non-useful images (i.e. keeping the raw files only for later processing). Regarding the computer power needed to calculate and generate the necessary files (e.g., point cloud, meshes, orthomosaic), in our particular case this increases exponentially in relation to the amount of data used (10,000 images in 2018, 4Tb of 3D data only) so this is a positive improvement. Currently, the project's Ubuntu-Linux cluster is able to manage most of the processing but is an expensive solution.

Acknowledgements: The authors express their gratitude to the organizers of the conference *Unlocking Sacred Landscapes II: Digital Humanities and Ritual Space*, Dr. Giorgos Papantoniou (University of Cyprus), Dr. Apostolos Sarris (Laboratory of Geophysical-Satellite Remote Sensing and Archaeo-environment, Crete), Dr. Christine Morris (Trinity College Dublin), and Dr. Athanasios Vionis (University of Cyprus), for giving us the opportunity to present some of the most recent results of a study on the episcopal district at Side.

The work was carried out by the Institute for the Study of Ancient Culture (IKAnt) of the Austrian Academy of Sciences in Vienna, Austria in cooperation with the Anadolu Üniversitesi at Eskişehir, Turkey excavation in Side and its head, Prof. Dr. H. S. Alanyalı.

References

Agisof LLC. (2017). *Split in chunks.py*. Retrieved from http://wiki.agisoft.com/wiki/Split_in_chunks.py

Auer, M., Agugiaro, G., Billen, N., Loos., & Zipf, A. (2014, 23–25 June) Web-based visualization and query of semantically segmented multiresolution 3D models in the field of Cultural Heritage. *ISPRS Annals of the Photogrammetry, Remote Sensing and Spatial Information Sciences*, (Vol. II–5). ISPRS Technical Commission V Symposium, Riva del Garda, Italy. Retrieved from https://www.isprs-ann-photogramm-remote-sens-spatial-inf-sci.net/II-5/33/2014/isprsannals-II-5-33-2014.pdf

Akca, İ. & Pülz, A. (2018). Side Piskoposluk Sarayi Çevresinde Yapilan Jeofizik Çalişmalar. *Kazı Sonuçları Toplantısı, 39*(2), 447–448.

Aktuğ, B., Lenk, O., Parmaksiz, E., Türkezer, A., Cingöz, A., Sezer, S., Simav, M., Direnc, A., & Özdemir, S. (2010). *National Report of Turkey-2010*. Geodesy Department, General Command of Mapping. Retrieved from https://www.researchgate.net/publication/284157489

Başçiftçi, F., Çağl, H., Ayten, T., Akkuş, S., Yalcin, B., & Şanlioğlu, I. (2006, October 8–13). *Determination of Geoid and Transformation Parameters By Using GPS On The Region of Kadınhanı In Konya*. Shaping the Change XXIII FIG Congress, Munich, Germany.

Buchwald, H. (1984). Western Asia Minor as a Generator of Architectural Forms in the Byzantine Period, Provincial Black-Wash or Dynamic Center of Production. *Jahrbuch der Österreichischen Byzantinistik* 34, 199–234.

Burns, J. H. R, Delparte, D., Gates, R. D., & Takabayashi, M. (2015). Integrating structure-from-motion photogrammetry with geospatial software as a novel technique for quantifying 3D ecological characteristics of coral reefs. *PeerJ* 3:e1077; DOI: 10.7717/peerj.1077

Campana, S., Sordini, & M., Remondino, F. (2008), Integration of geomatics techniques for the digital documentation of heritages areas, *Advances in Remote Sensing in the Archaeology and the Management of Cultural Heritage*. EARSEL Workshop (Rome, Italy), Rome, Aracne Retrieved from http://citeseerx.ist.psu.edu/viewdoc/download?doi=10.1.1.542.252&rep=rep1&type=pdf

Crawford, K. A. (2019). Rethinking Approaches for the Study of Urban Movement at Ostia. In: Verhagen P., Joyce J., Groenhuijzen, M. (Eds.), *Finding the Limits of the Limes.* Computational *Social Sciences* (pp. 313–327). Springer, Cham. DOI: 10.1007/978-3-030-04576-0_15

Ceylan, B. (2007). Episkopeia in Asia Minor. In L. Lavan & L. Özgenel & A. Sarantis (Eds.), Housing in Late Antiquity. From palaces to shops. *Late Antique Archaeology* 3.2 (pp. 169–193). Leiden - Boston: Brill.

Crooks, A., Hudson-Smith, A. & Patel, A. (2011). *Advances and Techniques for Building 3D Agent-Based Models for Urban Systems*, 1. 49–65. DOI:10.2174/978160805222611101010049

Dell'Unto, N., Landeschi, G., Leander Touati, A. M., Dellepiane, M., Callieri, M., & Ferdani, D. (2015). Experiencing ancient buildings from a 3D GIS perspective: a case drawn from the Swedish Pompeii Project. *Journal of Archaeological Method and Theory 23*(1), 73–94. DOI: 10.1007/s10816-014-9226-7

Doneus, M., Verhoeven, G., Fera, M., Briese, Ch., Kucera, M., & Neubauer, W. (2011). From deposit to point cloud – A study of low-cost computer vision approaches for the straightforward documentation of archaeological excavations, *Geinformatics FCECTU*, *6*, 81–88.

Eyice, S. (1957). Un baptistère byzantine à Side en Pamphylie. In *Proceeding of the V. CIAC*. Aix-en-Provence 1954. Studi di Antichità Cristiana 22 (III, pp. 577–583). Città del Vaticano, Paris: Pontificio Istituto di Archeologia Cristiana, Société d' Éditions Les Belles Lettres.

Eyice, S. (1957a). La ville byzantine de Side en Pamphylie. In *Proceeding of the X. CIEB*. Istanbul 1955 (pp. 130–133). Istanbul: Comite d' organisation du X. Congres International d' Études Byzantines.

Eyice, S. (1958). L´église cruciforme byzantine de Side en Pamphylie. Son importance au point de vue de l'histoire de l'art byzantine. *Anatolia* 3, 35–42.

Eyice, S. (1960). Side'nin Bizans devrine ait binalarının Sanat Tarihi bakımından değleri, V. *Türk Tarih Kongresi Ankara 1956* (pp. 53–60). Ankara.

Ersoy, N. (2011). Standardisation in engineering surveys in Turkey. *International Journal of the Physical Sciences, 6*(35), 8002–8006.

Faniel, I, Kansa, E., Whitcher Kansa, S., Barrera-Gomez, J., & Yekel, E. (2013). The challenges of digging data: a study of context in archaeological data reuse. *JCDL 2013 Proceedings of the 13th ACM/IEEE-CS Joint Conference on Digital Libraries*. Indianapolis, IN, USA — July 22 - 26, 2013. Retrieved from https://www.oclc.org/content/dam/research/publications/library/2013/faniel-archae-data.pdf

Foss, C. (1996). The Cities of Pamphylia in the Byzantine Age. In C. Foss (Ed.), *Cities, Fortresses and Villages of Byzantine Asia Minor* (pp. 1–62). Great Yarmouth: Variorum.

Gliwitzky, C. (2005). Die Kirche im sog. Bischofspalast zu Side. *IstMitt, 55*, 337–409.

Grau Mira, I. (2016) Archaeological surveys in areas with a high density of artefacts: Analysis and interpretation proposals, *Quaternary International*, 435, 1-10.

Heiskanen, W. A. & Moritz, H. (1967). *Physical Geodesy*. San Francisco: Freeman.

Hellenkemper, H. & Hild, F. (2004). *Lykien und Pamphylien,* Tabula Imperii Byzantini 8 = DenkSchrWien 320 (pp. 373–394). Wien: Verlag der Österreichischen Akademie der Wissenschaften.

Hernández Cordero, M. (2017). Geomatics approach to surveys for Late Antiquity buildings. The episcopal palace in Side, Turkey. *Archeologia e Calcolatori*. 28.2, 457–467.

Jaud, M., Passot, S., Le Bivic, R., Delacourt, C., Grandjean, P., & Le Dantec, N. (2016). Assessing the accuracy of high resolution digital surface models computed by PhotoScan® and MicMac® in sub-optimal survey conditions. *Remote Sensing*, *8*(60), 465. Retrieved from www.mdpi.com/journal/remotesensing

Kaderli, L. (2009). *Side Apollon, Athena tapınakları kutsal alanı ve Bizans bazilikaları, koruma yaklaşımı ve tarihi cevre değerlendirmesi* (unpubl. PhD thesis). Ankara: Ankara Üniversitesi, Mimar Sinan Güzel Sanatlar Üniversitesi, Fen Bilimleri Enstitüsü.

Kiliçoğlu, A. Direnç, A., Yildiz, H., Bölme, M, Aktuğ, B., Simav, M., & Lenk, O. (2010). Regional gravimetric quasi-geoid model and transformation surface to national height system for Turkey (THG-09). *Studia Geophysica et Geodaetica, 55*, 577–578. Retrieved from https://www.harita.gov.tr/yuksismod/images/egitim/87063c3b3376e86.pdf

Kowlessar, J., Benjamin, J., Moffat, I., & Van Duivenvoorde, W. (2019). Multi-scaler 3D modelling to reconstruct an experiential landscape: An example from a worker's cottage at Mount Dutton Bay, South Australia. *Journal of Archaeological Science: Reports, 23*, 478–489. Retrieved from https://doi.org/10.1016/j.jasrep.2018.10.026

Leica Geosystems, (2014). *System 1200 Newsletter*, No.11 Retrieved from https://www.google.com/url?sa=t&rct=j&q=&esrc=s&source=web&cd=1&ved=2ahUKEwj88Y3w2ODdAhVIqaQKHQuACgQQFjAAegQIBRAC&url=https%3A%2F%2Fsupport.smartnetna.com%2Fhc%2Fen-us%2Farticle_attachments%2F203871698%2FSystem1200_11_TwoStep_Coordinate_Systems.pdf&usg=AOvVaw0Yg_rrICnwEp23a23lkc4u

Leica Geosystems, (2016). *Leica Viva Series. Technical reference manual*, Version 1.0. Retrieved from https://leica-geosystems.com/products/total-stations/software/leica-geo-office

Leica Geosystems, (2018), *Leica Captivate Manual de Referencia Técnica*, 2018 v.2.0. Retrieved from geotop.com.pe/descargas/productos/832705_Leica_Captivate_TechRef_v2-0-0_es.pdf

Leica Geosystems, (2018a). *Leica Geo Office Online Help*, Version 8.4. Retrieved from https://leica-geosystems.com/products/total-stations/software/leica-geo-office

Lo Brutto, M. & Meli, P. (2012), Computer vision tools for 3D modelling in archaeology, *International Journal of Heritage in the Digital Era*, *1*(1), 1–6.

Mansel, A. M. (1963). *Die Ruinen von Side*, Berlin: De Gruyter.

Mansel, A. M. (1978). *Side 1947-1966 yilları kazıları ve arastırmalarının sonuçları*, Ankara: Türk Tarih Kurumu Basımevi.

Mercer, J. J., & Westbrook, C. J. (2016), Ultrahigh-resolution mapping of peatland icroform using ground based structure from motion with multiview stereo, *Journal of Geophysical Research: Biogeosciences.*, 121, 2901–2916, DOI: 10.1002/2016JG003478

Michelleti, N., Chandler, J. H., & Lane, S. (2015). Structure from motion (SFM) photogrammetry. In Cook, S. J., Clarke, L. E. & Nield, J. M. (Eds.), *Geomorphological Techniques* (Online Edition, Section 2.2.2). British Society for Geomorphology; London, UK. Retrieved from https://geomorphology.org.uk/sites/default/files/chapters/2.2.2_SfM.pdf

MicroSurvey Inc, (2018). *MicroSurvey FieldGenius v8 (2016-08-03)*. Retrieved from http://s3.microsurvey.com/fieldgenius/FieldGenius8/8.4/FieldGenius.pdf

Müller-Wiener, W. (1989). Bischofsresidenzen des 4.-7. Jhs. im östlichen Mittelmeerraum. In *Proceedings of the XI. CIAC 1986. Studi di Antichità Cristiana 41 = Collection de l' École Francaise de Rome 123* (I, pp. 651–709). Città del Vaticano – Paris: Pontificio Istituto di Archeologia Cristiana, Ecole francaise de Rome.

Nollé, J. (1993). *Side im Altertum. Geschichte und Zeugnisse I.* Inschriften griechischer Städte aus Kleinasien 43 = Side im Altertum I, Bonn: Habelt.

Nollé, J. (2001). *Side im Altertum. Geschichte und Zeugnisse II,* Inschriften griechischer Städte aus Kleinasien 44 = Side im Altertum II, Bonn: Habelt.

Ostrowski, W. & Hanus, K. (2016, July 12–19). Budget UAV systems for the prospection of small and medium scale archaeological sites. *The International Archives of the Photogrammetry, Remote Sensing and Spatial Information Sciences*, Volume XLI-B1, XXIII ISPRS Congress, Prague, Czech Republic.

Okiwelu, A., Ajuma, Ude, I., & Okwueze, E. (2011). Determination of Nigerian Geoid Undulations from Spherical Harmonic Analysis. *Applied Physics Research*, 3(1). Retrieved from http://www.ccsenet.org/journal/index.php/apr/article/view/9455

Peschlow, U. (2010). Mauerbau in krisenloser Zeit? Zu spätantiken Stadtbefestigungen im südlichen Kleinasien: Der Fall Side. In D. Kreikenbom et al. (Eds.), *Krise und Kult. Vorderer Orient und Nordafrika von Aurelian bis Justinian* (pp. 61–108). Berlin – New York: De Gruyter.

Piesker, K. (2017). Side. In P. Niewöhner (Ed.), *The Archaeology of Byzantine Anatolia. From the End of Late Antiquity to the Coming of the Turks* (pp. 294–301). Oxford: Oxford University Press.

Pirti, A. (2010). Evaluating the repeatability of RTK GPS. *Survey Review*, *43*(320), 23– 33. Retrieved from: https://doi.org/10.1179/003962611X12894696204984

Pülz, A. (2018). Ausgewählte Beispiele byzantinischer Wandmalereien in Side. In J. Drauschke, K. Kühtreiber, T. Kühtreiber, G. Scharrer-Liška, T. Via (Eds.), *Lebenswelten zwischen Archäologie und Geschichte*. Festschrift für F. Daim, Monographien des RGZM 150 (pp. 773–781). Mainz: Verlag des RGZM.

Ristow, S. (1998). *Frühchristliche Baptisterien,* JbAC Erg. Bd. 27. Münster: Aschendorffsche Verlagsbuchhandlung.

Roosevelt, C. H. (2014). Mapping Site-Level Microtopography with Real-Time Kinematic Global Navigation Satellite Systems (RTK GNSS) and Unmanned Aerial Vehicle Photogrammetry (UAVP), *Open Archaeology*, *1*(1), 29–53. DOI: 10.2478/opar-2014-0003

Ruggieri, V. (1995). Appunti sulla continuità urbana di Side, in Panfilia. *Orientalia Christiana Periodica, 61*(1), 95–116.

Ruggieri, V. (1995a). *L' architettura religiosa nell'Imperio Bizantino (fine VI–IX secolo)*, Messina: Rubbettino Editore.

Sanlioğlu, I., Maras, S. S., & Uysal, F. (2009, 3–8 May). Determination of Orthometric Heights with Real Time Kinematic Surveying, Konya Sample. *FIG Working Week 2009. Surveyors Key Role in Accelerated Development*. Eilat, Israel.

Scianna, A. & Villa, B. (2011). GIS applications in Archaeology. *Archeologia e Calcolatori, 22*, 337–363.

Schofield, W. & Breach, M. (2007), *Engineering Surveying, 6th Edition*, Oxford: Butterworth-Heinemann.

Tola, E., Knorr, S., Imre, E., & Alatan, A., (2005, October). Structure from motion in dynamic scene with multiple motions. *2nd Workshop on Immersive Communication and Broadcast Systems*, Berlin, Germany. Retrieved from https://infoscience.epfl.ch/record/150309/

Verhoeven, G., Doneus, M., Briese, C., & Vermeulen, F. (2012). Mapping by matching: A computer vision-based approach to fast and accurate georeferencing of archaeological aerial photographs, *Journal of Archaeological Science*, *39*, 2060–2070.

Wisconsin Department of Transportation, (2017). Real Time Kinematic (RTK) Surveys. Section 30 on Chapter 9. *Facilities Development Manual*. Retrieved from https://wisconsindot.gov/rdwy/fdm/fd-09-30.pdf

Yıldırım, Ş. (2013). *Side antik kentinin Bizans dönemi dini mimarisi,* (unpubl. PhD thesis). Eskişehir: Anadolu Üniversitesi Sosyal Bilimler Enstitüsü.

Yıldırım, Ş. (2017). Dating Dispute over the Cross-in-Square Church in the Episcopal, *Olba, 25*, 421–438.

Yilman, N. & Karaali, C. (2010). Comparison of global and local gravimetric geoid models in Turkey. *Scientific Research and Essays*, *5*(14), 1829–1839.

Yilmaz, S. (2013). *GNSS verilerinden hesaplanan elipsoid yüksekliklerinin atmosferik verilerle iyilestirilmesi*. Thesis. Aralik, Konya, Turkey. Retrieved from http://acikerisim.selcuk.edu.tr:8080/xmlui/handle/123456789/1032

Yilmaz, M., Turgut, B., Gullu, M., & Yilmaz, I. (2016). Evaluation of recent global geopotential models by GNSS/levelling data: internal Aegean region. *International Journal of Engineering and Geosciences (IJEG)*, 1(1), 18–23.